JOURNAL OF GEOPHYSICAL RESEARCH, VOL. 103, NO. D24, PAGES 32,141–32,157, DECEMBER 27, 1998

Discriminating clear sky from clouds with MODIS

Steven A. Ackerman,[1] Kathleen I. Strabala,[2] W. Paul Menzel,[3] Richard A. Frey,[2] Christopher C. Moeller,[2] and Liam E. Gumley[2]

Abstract. The MODIS cloud mask uses several cloud detection tests to indicate a level of confidence that the MODIS is observing clear skies. It will be produced globally at single-pixel resolution; the algorithm uses as many as 14 of the MODIS 36 spectral bands to maximize reliable cloud detection and to mitigate past difficulties experienced by sensors with coarser spatial resolution or fewer spectral bands. The MODIS cloud mask is ancillary input to MODIS land, ocean, and atmosphere science algorithms to suggest processing options. The MODIS cloud mask algorithm will operate in near real time in a limited computer processing and storage facility with simple easy-to-follow algorithm paths. The MODIS cloud mask algorithm identifies several conceptual domains according to surface type and solar illumination, including land, water, snow/ice, desert, and coast for both day and night. Once a pixel has been assigned to a particular domain (defining an algorithm path), a series of threshold tests attempts to detect the presence of clouds in the instrument field of view. Each cloud detection test returns a confidence level that the pixel is clear ranging in value from 1 (high) to zero (low). There are several types of tests, where detection of different cloud conditions relies on different tests. Tests capable of detecting similar cloud conditions are grouped together. While these groups are arranged so that independence between them is maximized, few, if any, spectral tests are completely independent. The minimum confidence from all tests within a group is taken to be representative of that group. These confidences indicate absence of particular cloud types. The product of all the group confidences is used to determine the confidence of finding clear-sky conditions. This paper outlines the MODIS cloud masking algorithm. While no present sensor has all of the spectral bands necessary for testing the complete MODIS cloud mask, initial validation of some of the individual cloud tests is presented using existing remote sensing data sets.

1. Introduction

The Moderate-Resolution Imaging Spectroradiometer (MODIS) is a keystone instrument of the Earth Observing System (EOS) for conducting global change research. The MODIS provides global observations of Earth's land, oceans, and atmosphere in the visible and infrared regions of the spectrum. Measurements at 36 wavelengths, from 0.4 to 14.5 μm, will allow investigators to study the Earth in unprecedented detail. Biological and geophysical processes will be recorded in the MODIS measurements on a global scale every 1 to 2 days. Many of the atmospheric and surface parameters require cloud free measurements. The MODIS cloud mask provides an estimate that a given MODIS field of view (FOV) is cloud free. It is a global level 2 product generated daily at 1 km and 250 m spatial resolutions.

MODIS measures radiances in two visible bands at 250 m spatial resolution, in five more visible bands at 500 m resolution, and the remaining 29 visible and infrared bands at 1000 m resolution. Radiances from 14 spectral bands (Table 1) are used in the MODIS cloud mask algorithm to estimate whether a given view of the Earth surface is unobstructed by clouds or optically thick aerosol and whether a clear scene is affected by cloud shadows.

The operational processing of MODIS requires adequate CPU capability, large file sizes, and easy comprehension of the output cloud masks. A note on each of these concerns follows.

1. The cloud mask algorithm lies at the beginning of the data processing chain for most MODIS products and thus must run in near real time, limiting the use of CPU intensive algorithms.

2. Storage requirements are a concern. The cloud mask is more than a yes/no decision. The cloud mask consists of 48 bits of output which include information on individual cloud test results, the processing path, and ancillary information (e.g., land/sea tag). The first eight bits of the cloud mask provide a summary adequate for many processing applications; however, some applications will require the full mask at 4.8 Gb of storage per day.

3. The cloud mask must be easily understood but provide enough information for wide use; it must be simple in concept but effective in its application.

This paper describes the approach for detecting clouds using MODIS observations and details the algorithms. Section 2 presents a very brief summary of some current global cloud detection algorithms and discusses the wavelengths used in the MODIS cloud mask algorithm. Section 3 discusses the approach employed by the algorithm. Section 4 details the input

[1]Department of Atmospheric and Oceanic Sciences, University of Wisconsin, Madison.
[2]Cooperative Institute for Meteorological Satellite Studies, University of Wisconsin, Madison.
[3]NOAA/NESDIS Advanced Satellite Products Team, University of Wisconsin, Madison.

Paper number 1998JD200032.
0148-0227/98/1998JD200032$09.00

Table 1. MODIS Spectral Band Number and Central Wavelength

Band	Wavelength, μm	Used in Cloud Mask
1 (250 m)	0.659	Y, (250 m and 1 km) clouds, shadow
2 (250 m)	0.865	Y, (250 m and 1 km) low clouds
3 (500 m)	0.470	N,
4 (500 m)	0.555	N, snow
5 (500 m)	1.240	Y, snow
6 (500 m)	1.640	Y, snow, shadow
7 (500 m)	2.130	N,
8	0.415	N,
9	0.443	N,
10	0.490	N,
11	0.531	N,
12	0.565	N,
13	0.653	N,
14	0.681	N,
15	0.750	N,
16	0.865	N,
17	0.905	N,
18	0.936	Y, low clouds
19	0.940	Y, shadows
26	1.375	Y, thin cirrus
20	3.750	Y, shadow
21/22	3.959	Y(21)/N(22), window
23	4.050	N,
24	4.465	N,
25	4.515	N,
27	6.715	Y, high moisture
28	7.325	N,
29	8.550	Y, midmoisture
30	9.730	N
31	11.030	Y, window
32	12.020	Y, low moisture
33	13.335	N,
34	13.635	N,
35	13.935	Y, high cloud
36	14.235	N,

Columns 3 (Y, yes; N, no) and 4 indicate if the channel is used in the cloud masking and its primary application.

and output of the algorithm. Section 5 describes some attempts at validation using current aircraft and space-borne sensors. Section 6 provides examples on how to interpret the cloud mask results. A summary is given in section 7.

2. Background

The MODIS cloud mask algorithm benefits from several previous efforts to characterize global cloud cover using satellite observations. The International Satellite Cloud Climatology Project (ISCCP) [*Rossow*, 1989; *Rossow et al.*, 1993; *Seze and Rossow*, 1991; *Rossow and Gardner*, 1993a, b] has developed cloud detection schemes using visible and infrared window radiances. The AVHRR (advanced very high resolution radiometer) processing scheme over cloud land and ocean (APOLLO) [*Saunders and Kriebel*, 1988; *Kriebel and Saunders*, 1988; *Gesell*, 1989] uses the two visible and three infrared bands of the AVHRR. The NOAA cloud advanced very high resolution radiometer (CLAVR) [*Stowe et al.*, 1991, 1994] adds a series of spectral and spatial variability tests to detect cloud. CO_2 slicing [*Wylie et al.*, 1994] characterizes global high cloud cover, including thin cirrus, using radiances in the carbon dioxide sensitive portion of the spectrum. *Frey et al.* [1995] developed a real-time, global algorithm for detecting cloud using collocated AVHRR and high-resolution infrared radiation

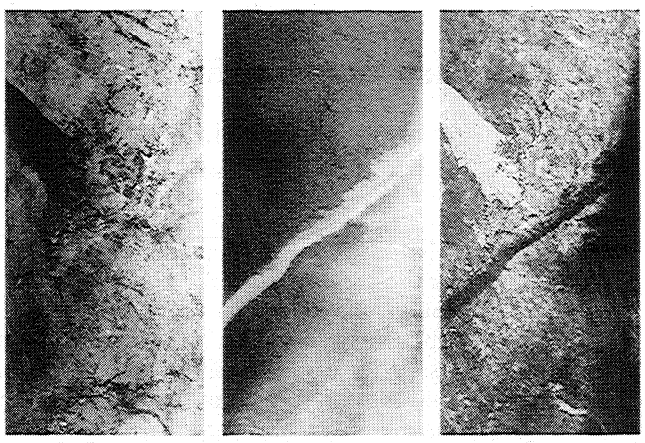

Figure 1. Three spectral images (0.66, 1.88, and 11 μm) taken from the MAS during the SUCCESS experiment (April 20, 1996). In the 11 μm image, dark is cold; in the vis/NIR images, white is high reflectance.

sounder (HIRS/2) observations. Many other algorithms have been developed for cloud clearing using the TIROS-N operational vertical sounder (TOVS); *Smith et al.* [1993] use collocated AVHRR and HIRS/2 to cloud clear, while *Rizzi et al.* [1994] base their work on the N^* approach developed by *Smith* [1968].

These algorithms have been used in global cloud climatologies over long time periods and thus have overcome some of the difficulties facing the MODIS cloud mask algorithm. A wide variety of scientists have discussed the physical basis behind each of the MODIS spectral tests, and applications to satellite or aircraft data are present in a variety of publications (*Ackerman et al.* [1997] include a reference list). The MODIS cloud mask algorithm builds on these past works by combining the different tests into a single unified algorithm at high spatial resolution.

The following notation is used in this paper: satellite-measured solar reflectance is r, and brightness temperature (equivalent blackbody temperature from the Planck radiance) is BT.

3. Algorithm

Clouds are generally characterized by higher reflectance and lower temperature than the underlying Earth surface. Simple visible and infrared window threshold approaches offer considerable skill in cloud detection; however, many surface conditions reduce cloud-surface contrast in certain spectral regions (e.g., bright clouds over snow and ice). Cloud types such as thin cirrus, low-level stratus at night, and small cumulus typically have low contrast with the underlying background. Cloud edges cause further difficulty since the instrument field of view will not always be completely cloudy or clear. The 36 spectral bands on the MODIS offer the opportunity for multispectral approaches to global cloud detection whereby many of these concerns can be mitigated.

Differences in the cloud-surface contrast across the spectrum can make a pixel appear cloudy in one spectral band and cloud free in another. To illustrate this point, Figure 1 presents three spectral images (histogram normalized) of a subvisual contrail taken from the MODIS airborne simulator (MAS) during the Subsonic Aircraft Contrail and Cloud Effects Spe-

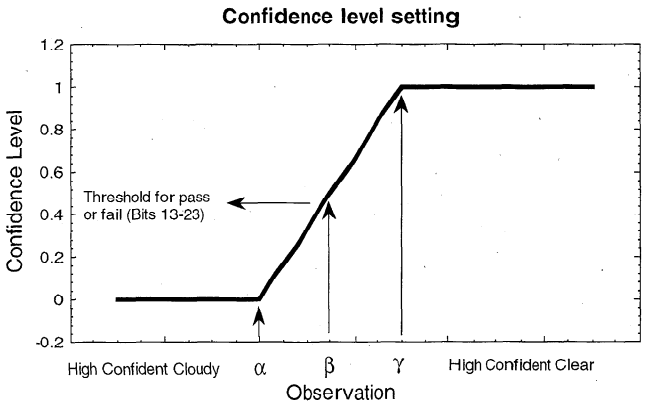

Figure 2. A graphical depiction of three thresholds used in cloud screening.

cial Study (SUCCESS). The left panel shows a MAS visible image at 0.66 μm, a spectral region found on many satellite sensors and commonly used by land surface classifications such as the vegetation index. The contrail is not apparent in this image. The right panel shows a MAS infrared window image at 11 μm (dark is cold, light is warm), again a spectral region found on many satellite sensors and commonly used to infer surface temperatures. There is very modest indication of a contrail, but it would be difficult to fully define its extent. The middle panel shows the MAS 1.88 μm spectral band which is located near a strong water vapor absorption band and is extremely sensitive to the presence of high-level clouds in daylight. The full contrail is very apparent. While the contrail seems to have little impact on visible reflectances, its effect is likely to be sufficient in the infrared window to affect estimates of surface temperature. In this type of scene, the cloud mask needs to provide information useful in both visible (no impact of contrail) and infrared (likely impact of contrail) applications. The 1.88 μm spectral band on MAS is expected to exhibit similar characteristics to the 1.38 μm spectral band to be available on MODIS, both are near a strong water vapor absorption band.

The MODIS cloud mask algorithm determines if a given pixel is clear by combining the results of several spectral threshold tests. All of the spectral cloud detection tests described below rely on thresholds. Thresholds are never global. There are always exceptions and the thresholds need to be interpreted carefully. For example, if the visible reflectance over the ocean (away from Sun glint) is greater than 6%, then the pixel is often identified as cloudy. However, it seems unrealistic to label a pixel with a reflectance of 6.1 as cloudy, and a neighboring pixel with the reflectance of 6.0 as noncloudy. Rather, as one approaches the threshold limit, the certainty or confidence in the cloud detection becomes less certain. Individual confidence values are assigned to the single-pixel tests and a final determination of whether the pixel is clear or cloudy is forged from the product of the individual confidence values.

Application of the individual spectral tests results in a confidence in the clear or cloudy determination for each FOV. Each test is assigned a value between zero and 1, where zero represents high confidence in cloudy conditions, and 1 represents high confidence in clear conditions, and the numbers in between represent increasingly less confidence in cloudy or clear conditions as 0.5 is approached. Figure 2 is a graphical representation of how a confidence level is assigned for a given spectral test. The abscissa represents the observation, and the ordinate the clear-sky confidence level. In this test, an observation greater than a value of γ is determined to be a high confidence clear scene and assigned a value of 1. An observation with a value less than α is cloudy and assigned a confidence level of zero. These high confidence clear and cloud thresholds, γ and α, respectively, are determined from previous studies, observations, and/or theoretical simulations. Observations between α and γ are assigned a confidence value between zero and 1 based on a linear function.

The MODIS cloud mask output includes the results from each individual test in binary form; either cloud (denoted by zero) or clear (denoted by 1) without the confidence in this particular test (denoted by values between zero and 1). This enables a user to inspect the results of a particular test and also allows the algorithm developer to track possible causes of cloud mask problems as they occur. The β value in Figure 2 is the pass/fail threshold for a test. Each test therefore has threshold values for pass/fail, high confidence pass, and high confidence fail. Some tests, such as the visible ratio test, identify cloud if the observations fall within a given range (e.g., $0.9 < r_{0.87}/r_{0.66} < 1.1$); for such a test there are three thresholds for each end of the range, six thresholds in all.

The uncertainty inherent in a threshold test is caused by instrument noise, inadequate characterization of the radiative properties of the Earth surface, and variations in atmospheric emission and scattering. The initial determination of cloud or clear within a MODIS FOV is an amalgamation of the confidence values for all the single-pixel tests. This initial determination dictates whether additional testing (e.g., spatial uniformity tests) is warranted to improve the confidence. The final determination assigns one of four levels: confident clear, probably clear, undecided, and cloudy. This approach attempts to quantify the confidence in the derived cloud mask for a given pixel. Thus the MODIS cloud mask algorithm produces more than a yes/no decision.

As discussed earlier, a variety of spectral observations enhance the chance of determining the presence of a cloud (e.g., Figure 1). The spectral tests in one spectral region can compensate for the problems with spectral tests in another spectral region. In the MODIS cloud mask algorithm, each spectral test is placed in one of five groups: (1) detecting thick high clouds with emitted radiation threshold tests using the brightness temperatures of BT_{11}, $BT_{13.9}$, and $BT_{6.7}$; (2) detecting thin clouds with brightness temperature difference tests $BT_{11} - BT_{12}$, $BT_{8.6} - BT_{11}$, $BT_{11} - BT_{3.9}$, and, $BT_{11} - BT_{6.7}$; (3) detecting low clouds with reflectance thresholds for $r_{0.87}$, $r_{0.65}$, and $r_{.936}$, reflectance ratio tests, and a brightness temperature difference test $BT_{3.9} - BT_{3.7}$; (4) detecting upper tropospheric thin clouds with a reflectance threshold test for $r_{1.38}$; and (5) cirrus sensitive brightness temperature difference tests $BT_{11} - BT_{12}$, $BT_{12} - BT_4$, and $BT_{13.7} - BT_{13.9}$. Tests within a group may detect more than one cloud type. Thresholds for each test can be found in the MODIS cloud mask Algorithm Theoretical Basis Document [*Ackerman et al.*, 1997].

Consider the example of daytime stratocumulus and cirrus clouds over oceans in regions without Sun glint. Stratocumulus clouds will likely be detected by the visible reflectance test, the reflectance ratio test, and the $BT_{11} - BT_{3.7}$. Very thin cirrus clouds would best be detected by the 1.38 μm and $BT_{11} - BT_{12}$ APOLLO tests, two tests which have difficulty detecting low-level clouds. It is important to realize that the cloud mask tests in the different groups are not independent of one another.

The task is to combine the different spectral cloud detection tests in the most effective manner. Several different methods of combining the individual tests have been investigated using a variety of data sets (see section 5). The technique described below produced consistent cloud detection.

3.1. Group I

This group detects thick high clouds with threshold tests using brightness temperatures in three infrared spectral bands, BT_{11}, $BT_{13.9}$, and $BT_{6.7}$. Infrared window thresholds, BT_{11}, are practical in certain conditions; however, they will vary with moisture content of the atmosphere. Over land, BT_{11} is further complicated by the fact that the surface emissivity varies appreciably with soil and vegetation type. Thus BT_{11} is used primarily to detect high, thick clouds, and thresholds are set accordingly. For example, clouds are likely to be present when BT_{11} is less than 270 K over tropical oceans. $BT_{13.9}$ provides good sensitivity to the relatively cold regions of the atmosphere because of CO_2 absorption. The same is true for $BT_{6.7}$ because of H_2O absorption. These spectral bands receive most of their radiation near 300 hPa, and only clouds above 500 hPa make strong radiance contributions; negligible contributions come from the Earth surface. Thus a threshold for $BT_{13.9}$ and $BT_{6.7}$ can isolate clouds above 500 hPa.

3.2. Group II

This group is focused on detection of thin clouds missed by Group I tests and includes brightness temperature difference tests $BT_{11} - BT_{12}$, $BT_{8.6} - BT_{11}$, $BT_{11} - BT_{3.9}$, and, $BT_{11} - BT_{6.7}$. Differences between BT_{11} and BT_{12} have been widely used for cloud screening with AVHRR measurements; this technique is often referred to as the split window technique.

Split window techniques have been used operationally for more than 6 years using 8.6 and 11 μm bandwidths from the NOAA 10 and NOAA 12 and the 11 and 12 μm bandwidths from the NOAA 11, with a coefficient independent of precipitable water [*Menzel et al.*, 1993; *Wylie et al.*, 1994]. A trispectral combination of observations at 8.6, 11, and 12 μm bands was suggested by *Ackerman et al.* [1990]. *Strabala et al.* [1994] further explored this technique by utilizing very high spatial resolution data from the MAS instrument. The premise of the trispectral technique is that within the 8 to 12 μm window, ice and water vapor absorption increase (at different rates) beyond 10.5 μm. $BT_{8.6} - BT_{11}$ greater than zero indicates cloud, while negative differences, over oceans, indicate clear regions. As atmospheric moisture increases, $BT_{8.6} - BT_{11}$ decreases, while $BT_{11} - BT_{12}$ increases.

Brightness temperature difference techniques using MODIS will be very sensitive to thin clouds if the surface emissivity and temperature are adequately characterized. For example, given a surface at 300 K and a cloud at 220 K, a cloud emissivity of .01 affects the sensed infrared window brightness temperature by 0.5 K. Since the anticipated noise equivalent temperature for many of the MODIS infrared window spectral bands is better than .05 K, the cloud detection capability will obviously be very good.

At night the difference between the brightness temperatures measured in the shortwave (3.9 μm) and in the longwave (11 μm) window regions can be used to determine if cloud is present; positive values of $BT_{3.9} - BT_{11}$ can be used to detect partial cloud or thin cloud within the sensor field of view. Small or negative differences are observed only for the case where an opaque scene (such as thick cloud or the surface) fills the field of view of the sensor. Negative differences occur over extended clouds due to the lower cloud emissivity at 3.9 μm. In daylight hours, solar reflection at 3.9 μm enhances the brightness temperature difference and is useful for detecting water clouds.

Distinguishing clear and cloudy conditions in polar regions during winter is challenging due to the cold surface temperatures. Recent analysis [*Ackerman*, 1996] has shown large negative values in $BT_{8.6} - BT_{11}$ during wintertime over the Antarctic Plateau and Greenland; these are indicative of a strong surface inversion and thus clear skies. In polar winter conditions this test is used in the MODIS cloud mask algorithm.

3.3. Group III

This group adds skill for detection of low clouds using solar reflectance tests that include reflectance thresholds ($r_{0.87}$, $r_{0.65}$, and $r_{.936}$), reflectance ratio tests, and $BT_{3.9} - BT_{3.7}$. These tests work well when there is a high contrast in the reflectance between the surface and the cloud, for example, clouds over dark vegetation and water. Group III tests complement Group I tests; Group III is sensitive to thick, low-level clouds, while Group I has difficulty with low clouds that have small thermal contrast between cloud and background. Spectral reflectance thresholds are routinely used in many cloud detection algorithms. A wide variety of thresholds exist in the literature, depending on surface type and solar and view angle geometry. The initial MODIS thresholds are given by *Ackerman et al.* [1997]. These thresholds are selected on the basis of the previous studies and data analyses described in section 5. It is likely that these thresholds will be slightly adjusted postlaunch.

Reflectance ratio tests utilize the difference in reflection from cloud versus Earth surface in wavelengths above and below 0.72 μm. Many Earth surfaces are less reflective below 0.72 μm than above, but clouds do not exhibit this behavior to any great degree. The reflectance ratio test uses the 0.87 μm reflectance divided by 0.66 μm reflectance ($r_{0.87}/r_{0.66}$). With AVHRR data, this ratio has been found to be between 0.9 and 1.1 in cloudy regions and outside in clear regions. New analyses [*McClain*, 1993] suggest that the minimum value may need to be lowered to about 0.8, at least for some cases. For cloud free ocean, the ratio is expected to be less than 0.75 [*Saunders and Kriebel*, 1988].

The shortwave infrared window bands at 3.7 and 3.9 μm are also used to detect the presence of clouds. Over land, longwave infrared window spectral variation in surface emissivity presents difficulties for brightness temperature difference tests. Shortwave infrared window spectral variation in surface emissivity is much smaller for some ecosystems, while spectral variation in cloud emissivity remains substantial. Thus brightness temperature differences between $BT_{3.7}$ and $BT_{3.9}$ are usually small in clear sky but larger in clouds. During the daylight hours the difference increases because of the increased solar energy at 3.7 μm.

3.4. Group IV

This group contributes good detection of high thin clouds. It consists of a single high-cloud test, and it is separated into a group of its own because no other test has been found to be as sensitive to the presence of thin cirrus. This relatively new approach to cirrus detection is suggested by the work of *Gao et al.* [1993]. A near-infrared band sensitive to H_2O absorption at 1.38 μm is used in reflectance threshold tests to detect the presence of thin cirrus cloud in the upper troposphere under

daytime viewing conditions. This cloud detection band lies near a strong water vapor absorption region; no upwelling-reflected radiance from the Earth's surface reaches the sensor when sufficient atmospheric water vapor is present (estimated to be about 0.4 cm precipitable water) in the FOV. Simple low- and high-reflectance thresholds can be used to separate thin cirrus from clear and thick (near-infrared cloud optical depth > ~0.2) cloud scenes.

3.5. Group V

Group V cloud detection tests also focus on detection of high thin cirrus. Group V tests consist of brightness temperature difference tests $BT_{11} - BT_{12}$, $BT_{12} - BT_4$, and $BT_{13.7} - BT_{13.9}$. The Group V tests are similar to those in Group II, but they are specially tuned to detect the presence of thin cirrus. $BT_{11} - BT_{12}$ is greater than zero in ice clouds due to the larger absorption at the longer wavelength in the infrared window. $BT_{12} - BT_4$ is less than zero in semitransparent cirrus as subpixel warm features dominate the shortwave window radiances within a FOV. $BT_{13.7} - BT_{13.9}$ is nominally positive in clear skies but goes to zero when viewing cirrus. The large differences between ground and cloud temperatures make these tests useful for thin cirrus detection.

3.6. Combining Group Results

The number of these groups and the number of tests in each group may expand postlaunch. The confidence indicator for a group G_i is the smallest of the confidence indicators for the individual tests within that group, F_i,

$$G_{i=1,5} = \min [F_i] \tag{1}$$

The cloud mask Q is then determined from the product of the minimum confidences of each group;

$$Q = \sqrt[N]{\prod_{i=1}^{n} G_i} \tag{2}$$

This approach is conservative in the estimation of clear sky; the cloud mask will err on the side of too many cloudy reports rather than too many clear-sky reports. If any test is highly confident that the scene is cloudy ($F_i = 0$), the confidence that the scene is clear will be $Q = 0$. The cloud mask reports four levels of confidence that the FOV has a nonobstructed view of the surface: confident clear ($Q > 0.99$), probably clear ($Q > 0.95$), undecided ($Q > 0.66$), and cloudy or obstructed ($Q \leq 0.66$).

4. Cloud Mask Inputs and Outputs

This section summarizes the input and output of the MODIS cloud mask algorithm. As indicated earlier, the cloud mask is a 48 bit word for each field of view. Since the thresholds are a function of scene domain, the cloud mask includes information about the processing path the algorithm has taken (e.g., land or ocean). The bit structure of the cloud mask is given in Table 2. The tests within a given processing path are presented in Table 3.

4.1. Input (Bits 3–7)

These input bits report the conditions with respect to day/night, Sun glint, snow/ice, and land/water; these data dictate the processing path taken by the cloud mask algorithm.

4.1.1. Bit 3, day/night flag. A combination of solar zenith angle and instrument mode (day or night mode) at the pixel latitude and longitude at the time of the observations is used to determine if a daytime or nighttime cloud-masking algorithm should be applied. Daytime algorithms are constrained to solar zenith angles less than 85°. If bit 3 is set to 1, daytime algorithms were executed.

4.1.2. Bit 4, Sun glint flag. Sun glint is assumed when the reflected Sun angle θ_r lies between 0° and 36°, where

$$\cos \theta_r = \sin \theta \sin \theta^\circ \cos \psi + \cos \theta \cos \theta^\circ \tag{3}$$

where θ° is the solar zenith angle, θ is the viewing zenith angle, and ψ is the relative azimuth angle.

4.1.3. Bit 5, snow/ice background flag. Some cloud detection tests (e.g., visible reflectance tests) are applied differently in the presence of snow or ice, which is inferred from the 500 m gridded MODIS snow/ice map. An abbreviated snow index [*Hall et al.*, 1995] has been incorporated into the cloud mask so that the cloud mask can update the snow/ice cover from the last 24 hours to accommodate synoptic changes. The snow/ice bit is set to a value of zero when the cloud mask processing algorithm assumes that snow or ice is present.

4.1.4. Bits 6 and 7, land/water background flag. Thresholds for the cloud mask spectral tests are adjusted according to the surface background (e.g., land, water, desert, or coast). On occasion, more than one flag could apply to a FOV; for example, the northwest coast of the African continent could be simultaneously characterized as coast, land, and desert. In such cases the flag that indicates the most important characteristic for the cloud-masking process is used. The flag precedence is as follows: coast, desert, land, or water. The desert classification is based on the 10-min Olson World Ecosystems data set. A U.S. Geological Survey (USGS) 1 km land/sea tag file is used for land/water discrimination.

4.2. Output (Bits 0, 1, 2, and 8–47)

The initial cloud mask results from combining single-pixel (1000 m FOV) multispectral tests. If the initial clear confidence level is inconclusive (between 0.05 and 0.95), then spatial uniformity tests are also applied. Over water the cloud mask is also examined for temporal consistency. This section outlines the spectral tests, placing little emphasis on actual thresholds. More discussion on preliminary thresholds is given by *Ackerman et al.* [1997]. Many of the single-pixel tests rely on thresholds that vary with surface emissivity, surface reflectance, atmospheric moisture, aerosol content, and viewing geometry. Initially, thresholds are specified on the basis of theoretical simulations, observations from existing instruments, and published works. Thresholds for MODIS data will require fine tuning when data are available.

The results of the individual tests are found in bits 13 through 23. They contain the binary (yes/no) summaries of tests that use 1 km observations or 250 and 500 m observations averaged to 1 km. These individual test results are useful for tracking causes of cloud mask problems and for isolating tests in user-preferred spectral regions. The β value in Figure 2 is the pass/fail threshold for each test. The number of spectral tests applied to a given field of view depends on the processing path. Table 3 lists the tests applied for each path. It is important to refer to this table when interpreting the test summaries; a value of zero can mean the pixel is clear or that the test was not performed.

Table 2. File Specification for 48-Bit MODIS Cloud Mask

	48 Bit Cloud Mask File Specification	
Bit Field	Description Key	Result
0	cloud mask flag	0 = not determined 1 = determined
1–2	unobstructed FOV quality flag	00 = cloudy 01 = uncertain clear 10 = probably clear 11 = confident clear
Processing path flags		
3	day/night flag	0 = night/1 = day
4	Sun glint flag	0 = yes/1 = no
5	snow/ice background flag	0 = yes/1 = no
6–7	land/water flag	00 = water 01 = coastal 10 = desert 11 = land
Additional information		
8	noncloud-obstruction flag (heavy aerosol)	0 = yes/1 = no
9	thin cirrus detected (near infrared)	0 = yes/1 = no
10	shadow found	0 = yes/1 = no
11	thin cirrus detected (infrared)	0 = yes/1 = no
12	spare (cloud adjacency)	(post launch)
	1 km Cloud Flags	
13	cloud flag, simple IR threshold test	0 = yes/1 = no
14	high cloud flag, CO_2 threshold test	0 = yes/1 = no
15	high cloud flag, 6.7 μm test	0 = yes/1 = no
16	high cloud flag, 1.38 μm test	0 = yes/1 = no
17	high cloud flag, 3.9–12 μm test	0 = yes/1 = no
18	cloud flag, IR temperature difference	0 = yes/1 = no
19	cloud flag, 3.9–11 μm test	0 = yes/1 = no
20	cloud flag, visible reflectance test	0 = yes/1 = no
21	cloud flag, visible ratio test	0 = yes/1 = no
22	cloud flag, near-IR reflectance test	0 = yes/1 = no
23	cloud flag, 3.7–3.9 μm test	0 = yes/1 = no
Additional tests		
24	cloud flag, temporal consistency	0 = yes/1 = no
25	cloud flag, spatial variability	0 = yes/1 = no
26–31	spares	
	250 m Cloud Flag—Visible Tests	
32	element(1,1)	0 = yes/1 = no
33	element(1,2)	0 = yes/1 = no
34	element(1,3)	0 = yes/1 = no
35	element(1,4)	0 = yes/1 = no
36	element(2,1)	0 = yes/1 = no
37	element(2,2)	0 = yes/1 = no
38	element(2,3)	0 = yes/1 = no
39	element(2,4)	0 = yes/1 = no
40	element(3,1)	0 = yes/1 = no
41	element(3,2)	0 = yes/1 = no
42	element(3,3)	0 = yes/1 = no
43	element(3,4)	0 = yes/1 = no
44	element(4,1)	0 = yes/1 = no
45	element(4,2)	0 = yes/1 = no
46	element(4,3)	0 = yes/1 = no
47	element(4,4)	0 = yes/1 = no

4.2.1. Bit 0, execution flag. Bit zero indicates whether the cloud mask algorithm was executed. The cloud mask will not be executed under some conditions (e.g., if all the radiance values used in the cloud mask are missing or out of acceptable range). If bit zero is set to zero, then the cloud mask algorithm was not executed.

4.2.2. Bits 1–2, unobstructed FOV quality flag. The confidence flag contained in bits 1–2 is the cloud mask summary; it conveys the strength of conviction that the cloud mask algorithm has an unambiguous conclusion for a given FOV. The final cloud mask determination is a combination of the confidences of all applied individual tests. Four levels of confidence

Table 3. MODIS Cloud Mask Tests Executed (✓) for a Given Processing Path

	MODIS Cloud Mask Test Layout for a Given Processing Path									
	Daytime Ocean	Nighttime Ocean	Daytime Land	Nighttime Land	Polar Day (snow)	Polar Night (snow)	Coastline Day	Coastline Night	Desert Day	Desert Night
BT_{11} (bit 13)	✓	✓								
$BT_{13.9}$ (bit 14)	✓	✓	✓	✓	✓	✓	✓	✓	✓	✓
$BT_{6.7}$ (bit 15)	✓	✓	✓	✓	✓	✓	✓	✓	✓	✓
$R_{1.38}$ (bit 16)	✓		✓		✓		✓		✓	
$BT_{3.7} - BT_{12}$ (bit 17)				✓		✓				✓
BT_{8-11} & BT_{11-12} (bit 18)	✓	✓	✓	✓			✓	✓	✓	✓
$BT_{3.7} - BT_{11}$ (bit 19)	✓	✓	✓	✓	✓	✓	✓	✓	✓	✓
$R_{.66}$ or $R_{.87}$ (bit 20)	✓		✓				✓			
$R_{.87}/R_{0.66}$ (bit 21)	✓		✓							
$R_{.935}/R_{.87}$ (bit 22)	✓		✓		✓		✓			
$BT_{3.7} - BT_{3.9}$ (bit 23)	✓		✓				✓		✓	
Temporal consistency (bit 25)	✓	✓								✓
Spatial variability (bit 25)	✓	✓								

are provided: 11 indicates confidence the FOV is clear, 10 indicates probably clear, 01 indicates it is undecided, and 00 indicates it is cloudy (see Table 2). Representations of bit fields are here ordered from right to left. Bit zero, or the right-most bit, is the least significant.

4.2.3. Bit 8, noncloud obstruction. Smoke from forest fires, dust storms over deserts, and other aerosols can obstruct the MODIS line of sight to the Earth surface; these FOVs may also be flagged as "cloud." Aerosol will be indicated (bit will be set to a value of zero) if simple spectral tests indicate the possible presence of aerosols. This is not an aerosol product; rather it is a flag that the MODIS may be viewing an aerosol-laden atmosphere.

Some simple tests have been incorporated to check if the FOV is contaminated with aerosol and not cloud. Negative values of $BT_{11} - BT_{12}$ are often observed over deserts and can be attributed to the presence of dust storms [*Ackerman*, 1997]; provided BT_{11} is warm, the noncloud obstruction bit is set to zero. The trispectral technique is used to flag potential volcanic aerosol contamination following *Ackerman and Strabala* [1994]. Thick smoke generated by forest fires are also flagged following the work of *King et al.* [1992].

4.2.4. Bit 9, thin cirrus (near infrared). MODIS added a unique spectral band, 1.38 μm, for the detection of thin cirrus [*Gao et al.*, 1993; *Ben-Dor*, 1994]. In the presence of sufficient atmospheric water vapor (estimated to be about 0.4 cm precipitable water) the Earth surface is obscured in this band. Since most of the atmospheric moisture is located low in the troposphere, high clouds appear bright and reflectance from low and midlevel clouds is mostly attenuated by water vapor absorption. Thus the 1.38 μm band is very sensitive to high thin clouds. If this bit is set to zero, thin cirrus was detected in threshold tests using the 1.38 μm band.

The MAS 1.88 μm band is being used to gain experience in detecting thin cirrus. Like the MODIS 1.38 μm band, the MAS 1.88 μm band is near a strong water vapor absorption band. Figure 1 demonstrates the potential utility of the 1.38 μm band. Given the sensitivity to thin high clouds, the new MODIS 1.38 μm band may detect more clouds than previous satellite algorithms have indicated. If the reflectance lies above the clear-sky threshold and below a thick cloud threshold, thin cirrus is indicated. In the MODIS cloud mask algorithm, it is possible to indicate both high confident clear and presence of thin cirrus. This approach was adopted because certain applications have little tolerance for cloud contamination, while others are much less sensitive.

4.2.5. Bit 10, shadows. The MODIS cloud-masking algorithm checks for shadows whenever the cloud mask indicates a clear FOV (bits 1 and 2 are greater than zero). The detection of cloud shadows has not been addressed adequately in the literature. Clear-sky scenes potentially affected by shadows can be computed given the viewing geometry, solar azimuth and zenith angles, cloud edges, and altitude. This is not feasible within the CPU restrictions of the MODIS cloud mask algorithm; in addition, the cloud altitude is not available. Therefore reflectance values at 0.94, 0.88, and 0.66 μm are used to detect cloud shadows over land. Using MAS data, it has been found that the following conditions indicate a shadow: $r_{0.94} < 0.12$ and $r_{0.87}/r_{0.66} >$ ocean threshold. Bit 10 is set to zero when shadows are suspected.

4.2.6. Bit 11, thin cirrus (infrared). A second thin cirrus test is necessary for nighttime conditions, when near-infrared measurements are not available. In addition, some IR algorithms will not be sensitive to thin cirrus flagged by the MODIS 1.38 μm band. The IR thin cirrus test applies brightness temperature differences to detect the presence of thin cirrus through the split window analysis of APOLLO and the trispectral approach of *Strabala et al.* [1994]. The IR thin cirrus bit 11 is set to zero when thin cirrus was detected using infrared bands.

4.2.7. Bit 12, adjacent clouds. If a pixel is clear, adjacent pixels will be searched for low confidence clear flags. If any are found, this adjacent cloud bit will be set to zero.

4.2.8. Bit 13, BT threshold. Several infrared window brightness temperature threshold and temperature difference tests have been developed; they are most effective at night for cold clouds over water and must be used with caution in other situations. The primary infrared test over the oceans checks if BT_{11} is less than 270 K; if so, the pixel fails the clear-sky condition. The α, β, and γ thresholds (see Figure 2) over ocean are 267, 270, and 273 K.

4.2.9. Bit 14, CO_2 spectral band test for high clouds. CO_2 slicing [*Smith and Platt*, 1978; *Wylie and Menzel*, 1989] can be used to determine effective cloud amount and height of high clouds. Because of CPU considerations, simplified tests using the CO_2 bands are used for high cloud detection.

Whether a cloud is sensed by a CO_2 band depends upon the atmospheric attenuation in that band and the altitude of the cloud. The spectral band at 13.9 μm provides good sensitivity to the relatively cold regions of the atmosphere. Only clouds above 500 hPa will have strong contributions to the radiance to space observed at 13.9 μm; negligible contributions come from the Earth's surface. Thus a threshold test for cloud versus ambient atmosphere is used to flag high clouds. Initial thresholds are based on HIRS/2 observations but will have to be modified to the MODIS spectral bands after launch.

4.2.10. Bit 15, H_2O spectral band test for high clouds. The MODIS spectral band at 6.7 μm provides good sensitivity to the relatively cold regions of the atmosphere and will see only clouds above 500 hPa. A threshold test for cloud versus ambient atmosphere is used to flag cloud-contaminated regions. Additionally, methods for using BT_{11} and $BT_{6.7}$ observations to detect upper tropospheric clouds have been developed [*Soden and Bretherton*, 1993]. These two bands in combination are especially useful for cloud detection over polar regions during winter. Under clear-sky conditions, strong surface radiative temperature inversions can develop during winter as a result of longwave energy loss from the surface through a dry atmosphere. In these conditions, IR bands sensing radiation from low in the atmosphere will often have a warmer brightness temperature than a window band. Large negative differences in $BT_{11} - BT_{6.7}$ exist over the Antarctic Plateau and Greenland during their respective winters [*Ackerman*, 1996]. This brightness temperature difference is an asset to detecting cloud free conditions over elevated surfaces in the polar night [*Ackerman*, 1996]. Clouds inhibit the formation of the inversion and obscure the inversion from satellite detection if the ice water path is greater than ~20 g m^{-2}. A positive difference of $BT_{11} - BT_{6.7}$ indicates cloud; differences more negative than -10°C produce high confidence of clear conditions. This test is applied only during the polar winter.

4.2.11. Bit 16, $R_{1.38}$ test. This test for cirrus cloud uses the MODIS 1.38 μm band [*Gao et al.*, 1993; *Ben-Dor*, 1994]. It complements the thin cirrus bit 9. The bit 16 test uses a larger reflectance threshold and thus flags thick cirrus not flagged by bit 9.

4.2.12. Bit 17, $BT_{3.7} - BT_{12}$ test. The shortwave minus longwave infrared window brightness temperature difference test is applied during the nighttime. This difference is useful for separating thin cirrus and cloud free conditions and is relatively insensitive to the amount of water vapor in the atmosphere [*Hutchison and Hardy*, 1995]. Bit 17 supplements bits 9, 11, and 16.

4.2.13. Bit 18, $BT_{11} - BT_{12}$ and $BT_{8.6} - BT_{11}$ test. Over regions where the surface emits like a gray body, spectral tests within various atmospheric windows can be used to detect the presence of a cloud. Differences between BT_{11} and BT_{12} are widely used for cloud screening with AVHRR measurements, often referred to as the split window technique. *Saunders and Kriebel* [1988] used $BT_{11} - BT_{12}$ to detect cirrus clouds: brightness temperature differences are greater over clouds than clear conditions. Cloud thresholds are set as a function of satellite zenith angle and BT_{11}. *Inoue* [1987] also used $BT_{11} - BT_{12}$ versus BT_{11} to separate clear from cloudy conditions. A trispectral combination of observations at 8.6, 11, and 12 μm was suggested for detecting clouds and inferring cloud properties by *Ackerman et al.* [1990]. *Strabala et al.* [1994] and *Frey et al.* [1995] further explored this technique. The basis of the split window and trispectral technique for cloud detection lies in the differential water vapor absorption that exists between different window bands (8.6 and 11 μm and 11 and 12 μm).

Brightness temperature difference testing can also be applied over land with careful consideration of variation in spectral emittance. For example, $BT_{8.6} - BT_{11}$ has large negative values over daytime desert and is driven to positive differences in the presence of cirrus.

4.2.14. Bit 19, $BT_{11} - BT_{3.9}$ test. The MODIS band at 3.9 μm measures radiances in the shortwave infrared window region near 3.5–4 μm. The difference between BT_{11} and $BT_{3.9}$ can be used to detect the presence of clouds. At night, negative values for $BT_{11} - BT_{3.9}$ indicate partial cloud or thin cloud within the MODIS FOV; $BT_{3.9}$ responds more to the warm fraction of the FOV than BT_{11} does. Small differences are observed only when opaque scenes (such as thick cloud or the surface) fill the FOV.

During the daylight hours, $BT_{11} - BT_{3.9}$ becomes a large negative with reflection of solar energy at 3.9 μm. This often reveals low-level water clouds. $BT_{11} - BT_{3.9}$ is not useful over deserts during daytime, because bright desert regions with highly variable emissivities tend to be classified incorrectly as cloudy. Experience indicates that the thresholds for detecting cloud with $BT_{11} - BT_{3.9}$ need to be adjusted according to ecosystem type.

4.2.15. Bit 20, visible reflectance test. This is a single-band threshold test that does well for discriminating bright clouds over dark surfaces (e.g., stratus over ocean) and poorly for clouds over bright surfaces (e.g., snow). The 0.66 μm (band 1) is used over land and coastal regions. The reflectance test is adjusted for viewing angle and is also applied in Sun glint regions as identified by the Sun glint test. The 0.88 μm reflectance test is applied over ocean scenes.

4.2.16. Bit 21, reflectance ratio test. The reflectances in 0.87 and 0.66 μm are similar over clouds and different over water and vegetation. Using AVHRR data, this ratio $r_{.87}/r_{.66}$ has been found to be between 0.8 and 1.1 in cloudy regions [*Saunders and Kriebel*, 1988; *McClain*, 1993]. The Global Environment Monitoring Index (GEMI) attempts to correct for atmospheric effects in deriving a vegetation index [*Pinty and Verstraete*, 1992; *Leprieur et al.*, 1996]. We have found this approach to be a better discriminator of cloud. The test

$$\eta(1 - 0.25\eta) - \frac{r_{0.87} - 0.125}{1 - r_{0.87}};$$

$$\eta = \frac{2(r_{0.66} - r_{0.87}) + 1.5r_{0.66} + 0.5r_{0.87}}{r_{0.66} + r_{0.87} + 0.5}$$

denotes cloudy conditions when η is less than a given threshold. This test does not work well over desert or coastal scenes and therefore is not executed in these ecosystems.

4.2.17. Bit 22, NIR reflectance test. Clouds that are low in the atmosphere are often difficult to detect with infrared techniques. The thermal contrast between clear sky and low cloud is small and sometimes undetectable. Reflectance techniques, including the reflectance ratio test, can be applied during daylight hours over certain ecosystems. Use of the MODIS band at 0.936 μm offers help under daytime viewing conditions. As documented by the work of *Gao and Goetz* [1991], this band is strongly affected by low-level moisture. When low clouds are present, they obstruct the low-level moisture and hence increase the reflectance at 0.936 μm.

4.2.18. Bit 23, $BT_{3.7} - BT_{3.9}$ test. The spectral variation in surface emissivity can present difficulties in applying the

brightness temperature difference tests using $BT_{3.7}$, BT_{11}, and BT_{12}. Brightness temperature differences between $BT_{3.7}$ and $BT_{3.9}$ reduce this problem for some ecosystems. During the daylight hours $BT_{3.7} - BT_{3.9}$ increases because of the increased solar energy at 3.7 μm.

4.2.19. Bit 24, temporal consistency. Composite clear-sky infrared observations over ocean surfaces will be used to increase confidence of clear/cloudy scene identifications. Composite maps have been found to be very useful by ISCCP. The MODIS cloud mask will use composite maps but probably rely on them to a lesser extent since the advantages of higher spatial resolution and more spectral bands will change the application and the need.

The lack of reflected solar energy during nighttime processing has the overall effect of decreasing confidence in the cloud mask output. Some confidence can be restored by using clear-sky data maps. Cloud-cleared 11 μm brightness temperatures from daytime processing are used as input to the nighttime cloud-masking algorithm. Single-pixel, high confidence ($Q > 0.95$) clear-sky values of brightness temperatures, obtained by the MODIS cloud-masking algorithm during daylight hours when solar reflectance is available, will be incorporated into an 8-day composite equal-area grid at 25 km resolution. The composite data set will be updated after each day is processed, so clear-sky observations from day 1 of the previous eight days will be eliminated and those from the current day will be added. The 8 day cycle was chosen because seasonal changes in ocean temperature will be adequately represented and because 8 days is equal to the precession period of high-inclination polar orbiting satellites. Mean, maximum, and minimum values of BT_{11} will be made available to the nighttime cloud mask algorithm.

Even though the final output of the cloud mask is given by only four confidences of nonobstructed surface ($Q > 0.99$, $Q > 0.95$, $Q > 0.66$, and $Q < 0.66$), internally, the algorithm has four additional confidence levels ($Q > 0.34$, $Q > 0.05$, $Q > 0.01$, and $Q \leq 0.01$). The algorithm assigns a confidence value to each single pixel. After an initial assessment the BT_{11} of each pixel will be compared to the daytime composite values from the appropriate grid box. This comparison is designed to detect inconsistencies between the instantaneous pixel IR measurement and an expected confidence value (for that measurement) based on the previous eight days of data. If the observed value is less than the minimum composite value, then the pixel confidence is lowered by two levels. If the observation is greater than or equal to the minimum but less than the mean, then the confidence is downgraded by only one level. In the same way, confidences are raised when instantaneous brightness temperatures are greater than the mean and/or maximum composite values. This method allows for lessened confidence in the basic algorithm when applied in the absence of solar reflection but also recognizes the validity of the IR threshold tests. It also has the effect of eliminating many midrange confidences and adding them to either higher or lower percentage categories.

4.2.20. Bit 25, infrared window radiance spatial uniformity. The infrared window spatial uniformity test (applied on 3×3 pixel segments) is effective over water but is used with caution in other situations. Most ocean regions are well suited for spatial uniformity tests; such tests may be applied with less confidence in coastal regions or regions with large temperature gradients (e.g., the Gulf Stream). The MODIS cloud mask currently uses a spatial variability test over oceans and large lakes. The tests are used to modify the confidence of a pixel being clear. If the confidence flag of a pixel is between 0.05 and 0.95, the variability test is implemented. If the difference between the pixel of interest and all of the surrounding pixel brightness temperatures is less than 0.5°C, the scene is considered uniform, and the confidence is raised one confidence level.

Surface temperature variability, both spatial and temporal, is larger over land than ocean, making land scene spatial uniformity tests difficult. Therefore they are not executed over land.

4.2.21. Bits 26 and 31, spare bits. These spare bits are reserved for future developments.

4.2.22. Bits 32–47, 250 m resolution flags. The 250 m mask will be based on reflectance tests using only the bands at 0.66 and 0.88 μm (see tests for bits 20 and 21). The results are a simple yes/no decision. The 250 m cloud mask will be collocated within the 1000 m cloud mask in a fixed way; of the 28 250 m pixels that can be considered located within a 1000 m pixel, the most centered 16 will be processed for the cloud mask. The collocation of the 250 m pixels within the 1 km FOV is discussed by *Ackerman et al.* [1997]. Since only two bands will be used to generate the 250 m mask, it is expected to be of lower quality than the 1 km product. Furthermore, this high-resolution mask will only be generated in daytime, Sun glint free oceans, and nondesert regions. The cloud mask at 250 m resolution does not incorporate the results from the 1 km resolution tests.

It is possible to infer cloud fraction in the 1000 m field of view from the 16 visible pixels within the 1 km footprint. The cloud fraction would be the number of zeros divided by 16. This would not be advisable in some situations, such as clouds over snow.

5. Validation

This section presents some of the strengths and weaknesses of the MODIS cloud mask algorithm. Validating cloud detection is difficult [*Ackerman and Cox*, 1981; *Rossow and Garder*, 1993b; *Baum et al.*, 1995]. Two important steps in validation are image interpretation and quantitative analysis. In image interpretation, an analyst conducts a validation through visual inspection of the spectral, spatial, and temporal features in a set of composite images. Visual inspection is an important first step in validating any cloud mask algorithm. The analyst uses knowledge of and experience with cloud and surface spectral properties to identify obvious problems. However, visual inspection provides poor quantitative evaluation. More quantitative validation can be attained through direct pixel-by-pixel comparison with collocated ground or instrument platform-based observations, such as lidar. While this approach provides quantitative accuracy, it possesses the problem that the two measurement systems often observe different cloud properties [*Baum et al.*, 1995]. This section provides some validation examples using image interpretation and quantitative analysis.

In preparation for a MODIS day-1 cloud mask product, observations from the MODIS airborne simulator (MAS) [*King et al.*, 1996], AVHRR, and the HIRS/2 [*Frey et al.*, 1995] are being used to develop a multispectral cloud mask algorithm. The AVHRR and HIRS/2 instruments fly on the NOAA polar orbiting satellites providing global coverage, while the MAS flies onboard the NASA high-altitude ER-2 aircraft collecting 50 m resolution data in 50 visible and infrared spectral bands across a 37 km swath. The basic data sets

Table 4. Data Used in Development of MODIS Cloud Mask Algorithm and Their Characteristics

Data Set	Advantages	Disadvantages
AVHRR LAC (5 bands)	similar spatial resolution; readily available	no global coverage
AVHRR GAC (5 bands)	global coverage; readily available	4 km footprint
Collocated HIRS/AVHRR (19/5 bands)	many MODIS-like IR bands; collocation of smaller pixels within larger footprint	large HIRS/2 FOV; gaps between HIRS footprints
MAS (50 bands)	most MODIS like data set; high spatial and spectral resolution	no global coverage

currently being used to develop the cloud mask algorithm are listed in Table 4, as well as brief descriptions of the advantages and disadvantages of each data set. This section provides examples of the MODIS cloud mask algorithm approach using AVHRR and MAS observations.

5.1. Image Interpretation

Figure 3 shows NOAA-14 AVHRR global area coverage (GAC) observations. The left panel is the 0.6 μm image and the middle panel is the 11 μm image. The scene is over the tropical Pacific Ocean. The resulting cloud mask output file is represented in the right panel. The legend is as follows: black, confident of clear (bits 1–2 equal 11); dark gray, probably clear (bits 1–2 equal 10); light gray, undecided (bits 1–2 equal 01); and white, low confidence of clear (bits 1–2 equal 00). Notice that the confidence in the clear-sky scene tends to drop over the Sun glint region (see visible image), as it is difficult to detect clouds in areas affected by Sun glint. The multispectral advantage of MODIS should improve clear-sky detection capabilities in Sun glint regions. Other AVHRR cloud mask examples can be found at http://cimss.ssec.wisc.edu/modis/cldmsk/ack.

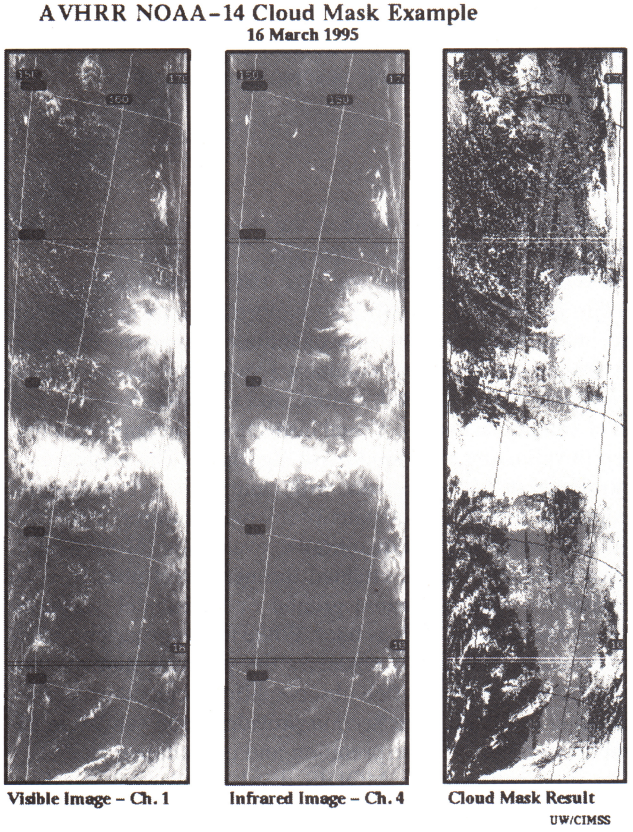

Figure 3. An example of the cloud mask derived from AVHRR data for a scene over the Pacific Ocean (right-hand panel), together with images from two of the AVHRR bands used in generating the mask. The legend is as follows: black is high confidence of clear (bits 1–2 equal 11), dark gray is probably clear (bits 1–2 equal 10), light gray is uncertain (bits 1–2 equal 01), and white is cloudy (bits 1–2 equal 00).

AVHRR global data sets are being used to develop clear-sky composite maps. In this simple and straightforward implementation of clear-sky composite maps, there are several common problems that are not explicitly addressed. One problem is changing of air masses, which occurs regularly in midlatitudes and often at higher frequency than 8 days. Changes in lapse rate and total column precipitable water amounts can lead to invalid composite values for any given day. However, since the entire algorithm is tuned as much as possible (via threshold test confidence intervals) to detection of clear sky, as opposed to cloudy sky, it is anticipated that errors of this kind will not produce very many false clear-sky identifications. Another possible source of error is due to limb darkening. Problems can occur when comparing instantaneous brightness temperatures from large viewing zenith angles with composites taken primarily from near-nadir views and vice versa. In the former case, lessened confidences near the limb are possible, but this is a general problem in remote sensing with scanning instruments. Discriminating clear sky from clouds is more difficult at limb view angles even for expert image analysts. In the latter case, the same argument is made as before, that the cloud mask algorithm is (properly) tuned toward maximum cloud detection, so it is more likely to falsely identify a cloud than clear sky.

The clear-sky composite was tested using AVHRR GAC data collected during July 1985 in the region encompassing 60° north to 40° south latitude and 40° west to 20° east longitude. This area was chosen because it contains a large range of ocean temperatures as well as atmospheric and cloud conditions. The AVHRR cloud detection with five spectral bands is necessarily limited compared to that of the MODIS with 14 spectral bands. However, because orbital characteristics, coverage, and spatial resolution are comparable, AVHRR was chosen as the input for the test.

The test was organized as follows: Daytime clear-sky ocean brightness temperatures were collected during the first eight days of the month. Independently, nighttime ocean clear-sky

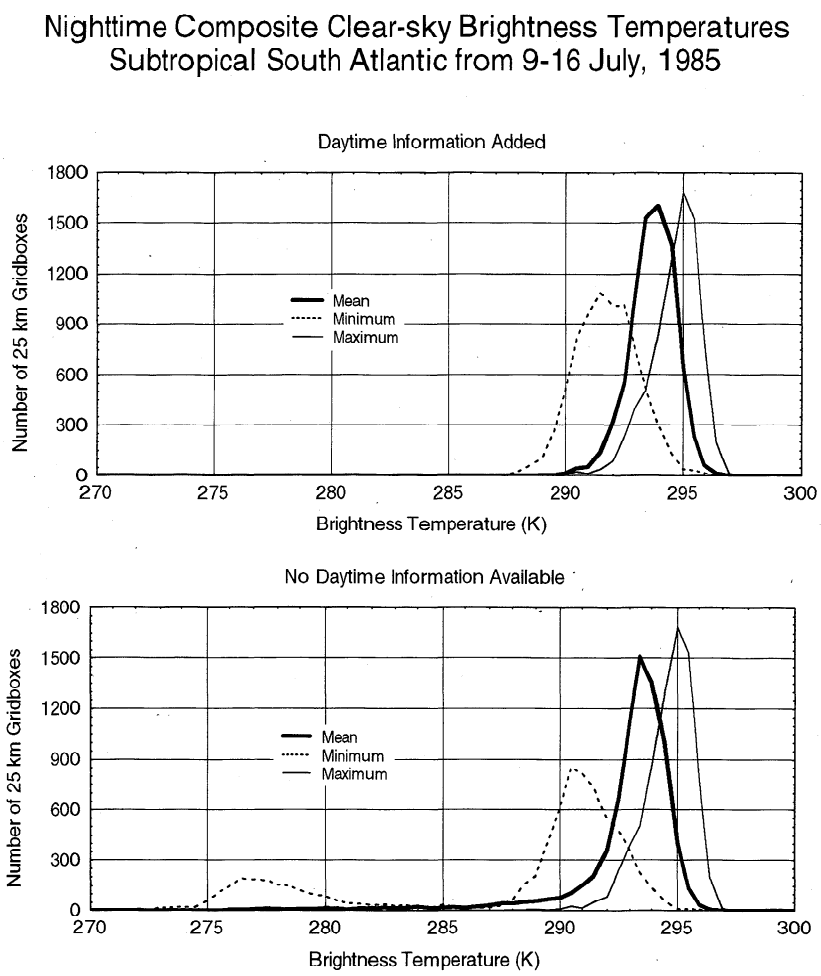

Figure 4. Distribution of BT_{11} in clear-sky conditions with daytime observations (top) and without (bottom).

results were collected for the second eight days of the month. Daytime results were also collected during the second eight days. Nighttime observations from the second eight days were processed again but, this time, using daytime brightness temperature information.

Figure 4 shows histograms of the grid box means, minima, and maxima for the second 8 day period from the region within 0° to 30° south latitude and 10° to 30° west longitude. Low-level clouds are the predominant type in this part of the world in July and are often difficult to detect at night. Note the skew of the mean and minimum histograms toward colder temperatures when no daytime information is available (bottom). This generally indicates cloud contamination. The secondary maximum which peaks between 275 and 280 K in the minimum histogram indicates some persistent low cloud feature which went consistently undetected by IR threshold and 11 μm variability tests. The top graph shows the improvement after adding temperature information from daytime processing. All three of these histograms show a more or less normal distribution expected from clear-sky measurements. Also note that the maximum temperature histograms are very nearly identical in both graphs, again as expected.

The cloud mask algorithm has been applied to numerous MAS scenes. One example is an image composed of different cloud types observed during SUCCESS on April 21, 1996, at ~2029 UTC (Figure 5). The top left image is the resulting cloud mask image. The next three images are from the MAS 11, 0.66, and 1.88 μm spectral bands. Visual inspection demonstrates that the cloud mask appears to accurately flag the cloudy and clear pixels. The bottom panels of the figure indicate the results from four spectral tests, each in different groups. In these four panels, white regions present pixels that exceed the β threshold of that particular spectral test. The $BT_{13.9}$ test flags the coldest pixels as cloudy but misses the low-level clouds and much of the thin cirrus clouds. The $BT_{11} - BT_{3.9}$ test captures most of the low-level clouds and much of the thin cirrus. The visible ratio test also captures much of the cloud scene. Careful inspection of the $BT_{11} - BT_{3.9}$ and visible ratio test images indicates some differences in the cloud detection from these two tests. The final image is the $r_{1.88}$ reflectance test, which captures all of the cirrus but misses the low-level clouds. The final cloud mask result is a combination of these spectral tests. While several of the tests overlap in the regions flagged as cloudy (i.e., they all detect the thick cirrus cloud), there are regions where certain tests flag clouds which others miss. This is the advantage of using a variety of spectral tests. The strength of an individual test is a function of the cloud type, the underlying surface, and the atmospheric temperature and moisture structure.

Figure 6 is another example of the cloud mask using MAS data as input. The top three panels are the 0.66, 1.88, and 1.6 μm images made at ~1945 UTC on April 26, 1996, over Kan-

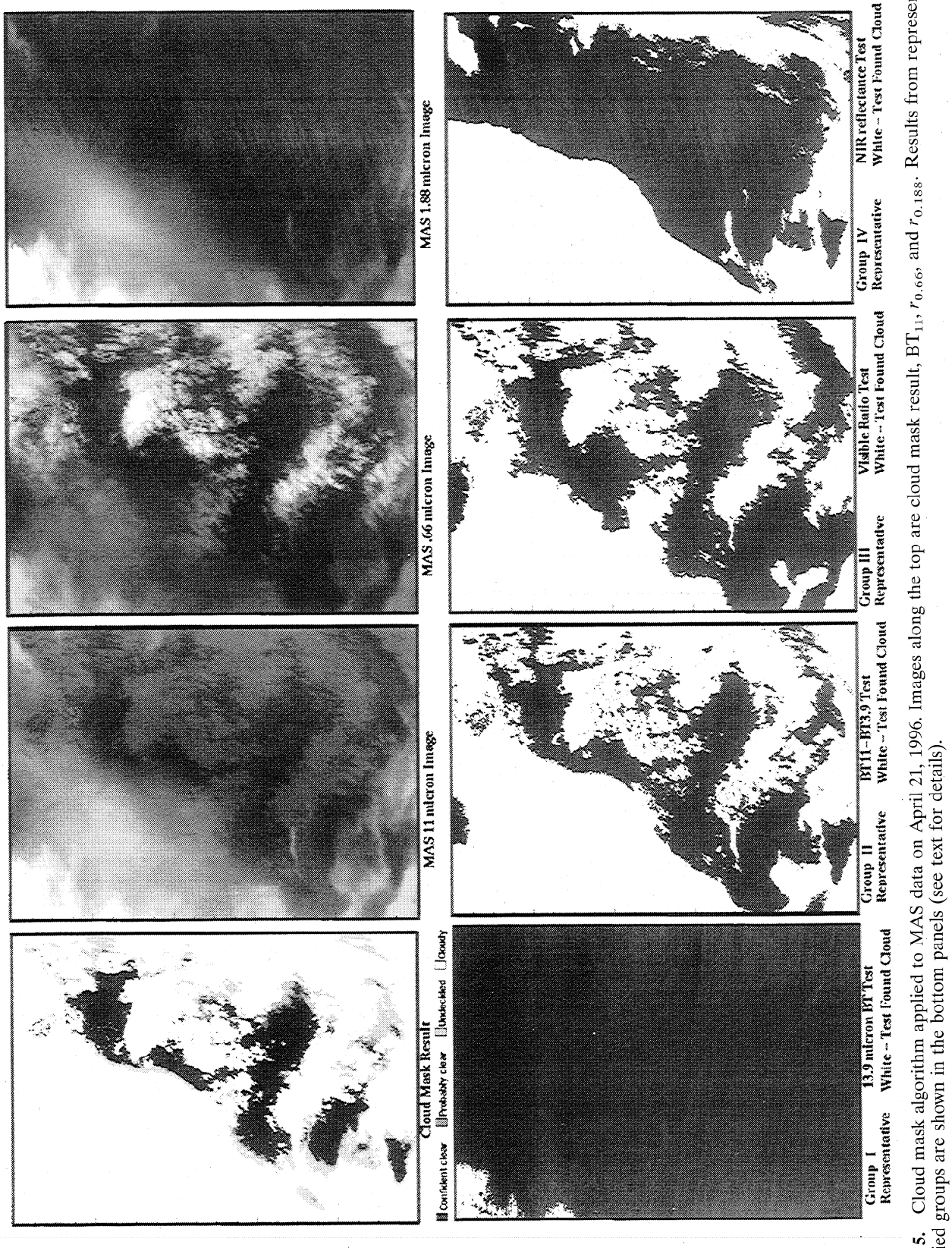

Figure 5. Cloud mask algorithm applied to MAS data on April 21, 1996. Images along the top are cloud mask result, BT_{11}, $r_{0.66}$, and $r_{0.188}$. Results from representative tests in applied groups are shown in the bottom panels (see text for details).

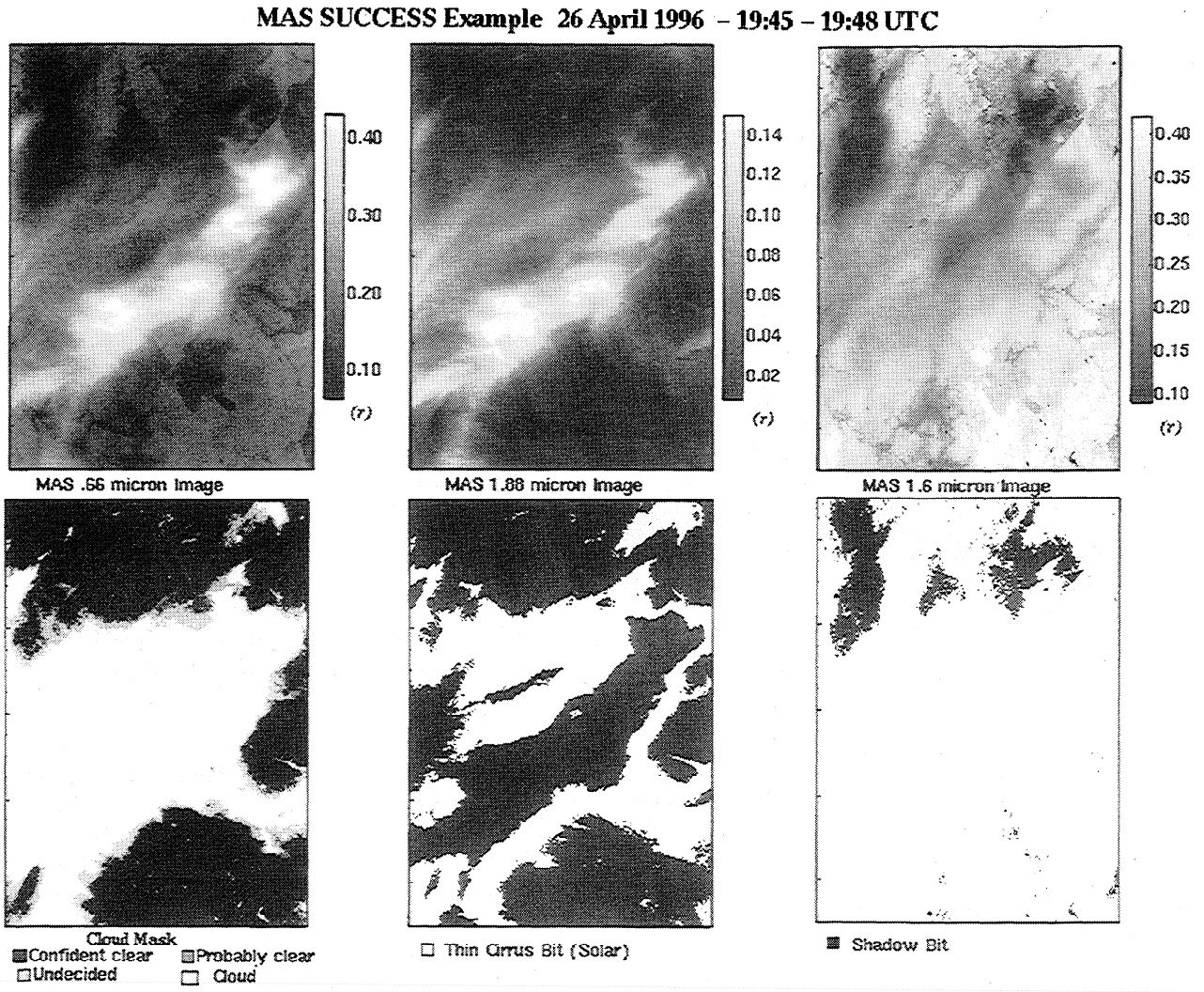

Figure 6. Example of cloud mask algorithms applied to MAS data on April 26, 1996. The top panels are MAS images at 0.66, 1.88, and 1.6 μm. The bottom images show the final mask, thin cirrus mask, and the shadow mask.

sas, United States. The 0.66 μm image indicates the presence of a cirrus band extending diagonally across the image. The 1.88 μm image shows regions of thin cirrus around the thicker cirrus. The low reflectance regions in the 1.6 μm image are cloud shadows. The final cloud mask result is displayed in the bottom left panel. Most of the scene is flagged as high or low confident clear; very few pixels are labeled as undecided. Inspection of the cloud mask image with the spectral images indicates the algorithm is detecting most of the cloud regions. The MODIS cloud mask also indicates regions of thin cirrus. This is demonstrated in the bottom middle panel of Figure 6, where white regions indicate the presence of thin cirrus. The surface is distinguishable in the 0.66 μm image where much of the image is flagged as thin cirrus. The thin cirrus flag (optical depth less than ~0.1) is set for regions where land property retrieval algorithms should incorporate a cloud correction in addition to the atmospheric correction. The bottom right-hand panel of Figure 6 demonstrates the results of the shadow algorithm. The shadow test captures most of the cloud shadows.

Figure 7 is an example of a scene that has very different meteorological conditions than the previous ones. The observations were taken over North Dakota on February 2, 1997, at ~1725 UTC. The left panel is the MAS 0.66 μm image and indicates the presence of a cloud in the top left-hand portion of the image with much of the area covered with snow. The 1.88 μm image (middle panel) indicates that much of the region is also covered by thin cirrus. Detection of thin cirrus is lacking in the 0.66 μm image, yet consistent with lidar measurements. The cloud mask algorithm flagged most of the region as low confidence clear and thin cirrus contaminated.

5.2. Comparison With Collocated Observations

Image visualization is an important component of validating any cloud detection algorithm. Additional validation includes comparison with active and passive measurements of clouds. In anticipation of future MODIS cloud mask verification efforts, a prototype methodology has been developed using the AVHRR cloud mask product. Three complete AVHRR GAC orbits are processed daily, using the previous day's level-1b data as input. Daytime coverage includes the Amazon Basin, eastern North America, the Saudi Arabian peninsula, and central Europe. Hourly surface observations from 10 manned weather stations in North America (ranging in latitude from 30°N to 70°N), closest in time to the satellite measurement, are

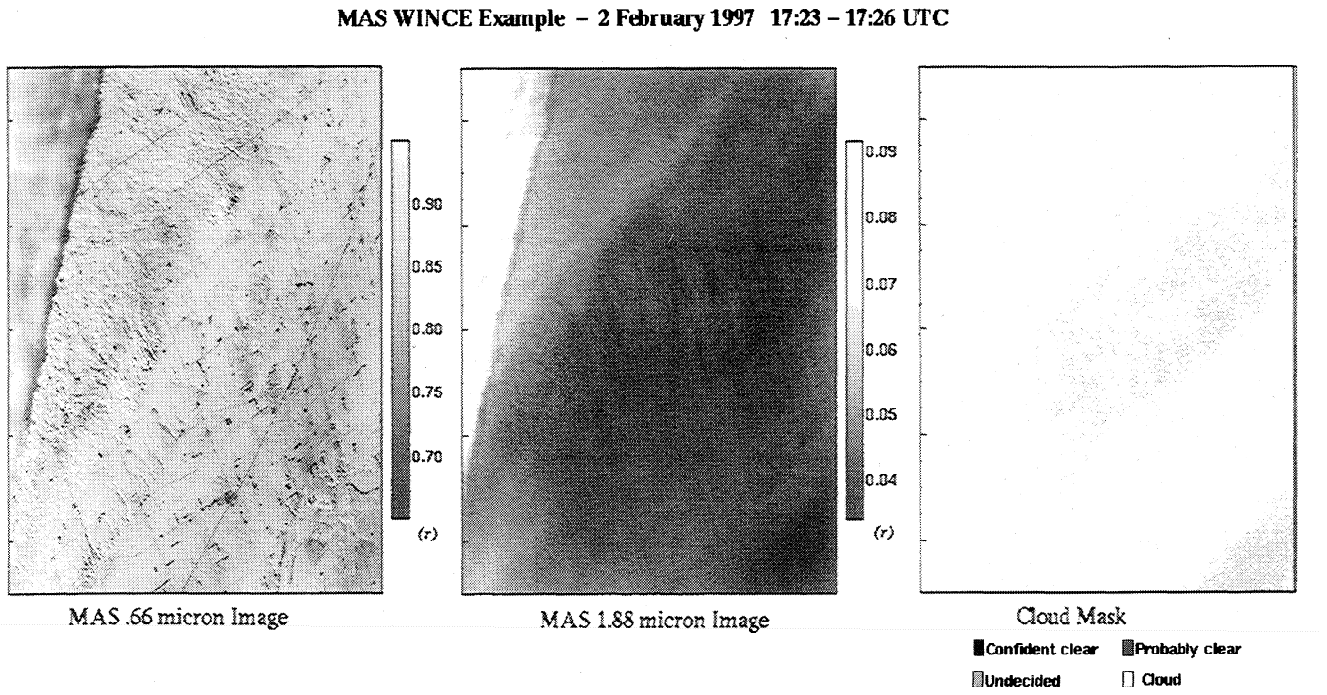

Figure 7. Example of the cloud mask algorithm applied to a winter scene on February 2, 1997.

collected and compared to the cloud mask output. Figure 8 is a 3-D histogram that compares the surface observation with the closest AVHRR pixel for August and September 1997. Weather station cloud reports are plotted on the x axis and the satellite-derived clear-sky confidence level on the y axis. The z axis is the frequency of occurrence in each category. Surface observations of cloudiness are reported as "clear," "few," "scattered," "broken," and "overcast." Cloud coverage for these categories is 0/8, 1/8–2/8, 3/8–4/8, 5/8–7/8, and 8/8, respectively. The cloud mask is generally doing a satisfactory job, particularly for clear skies. This is a result of the conservative nature of the cloud mask, where only very high confidence pixels are designated as clear. As one sees more clouds from the ground, the cloud mask confidence for seeing clear sky diminishes, as expected.

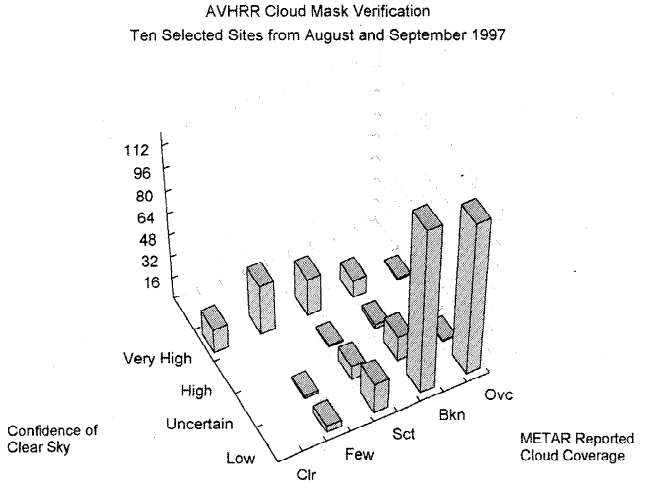

Figure 8. Comparison of surface cloud reports and AVHRR cloud mask results. Note the good agreement in clear as well as broken and overcast skies.

To quantify the MAS cloud mask algorithm performance, comparisons are made with observations from the Cloud Lidar System (CLS) [*Spinhirne and Hart*, 1990]. During the SUCCESS, the MAS flew along with the lidar. The CLS algorithm detects a maximum of five cloud top and cloud bottom altitudes based upon the backscatter signal. Each collocation consists of the CLS cloud product and ~250–300 MAS pixels. The percentage of pixels labeled confident clear, probably clear, uncertain, and low confident clear are determined for each collocated scene. The CLS observations are divided into three categories: clear, no cloud was detected by the lidar; thin cloud, cloud boundary was detected, but a surface return signal was also received; thick cloud, cloud boundary was detected with no surface return signal. Histograms of the percentage of pixels in a given confidence interval are plotted for each CLS cloud type category (see Figure 9). Nearly all of the CLS labeled clear scenes are identified as high confident clear by the MAS cloud mask algorithm. Essentially all of the CLS labeled thick cloud scenes are labeled as cloudy by the MAS cloud mask. A majority of the thin cloud cases are labeled as either confident clear or cloudy by the MAS cloud mask algorithm. Differences between those scenes labeled clear and those classified cloudy are related to the cloud thickness. A more detailed analysis is required for verification of these thin clouds. Such a study is in progress. Also encouraging from this comparison is that few of the scenes are labeled as uncertain. Visualization of the cloud mask indicates that many of these scenes occur near cloud edges.

6. Examples

This section provides examples of how to interpret output from the cloud mask algorithm for a particular application.

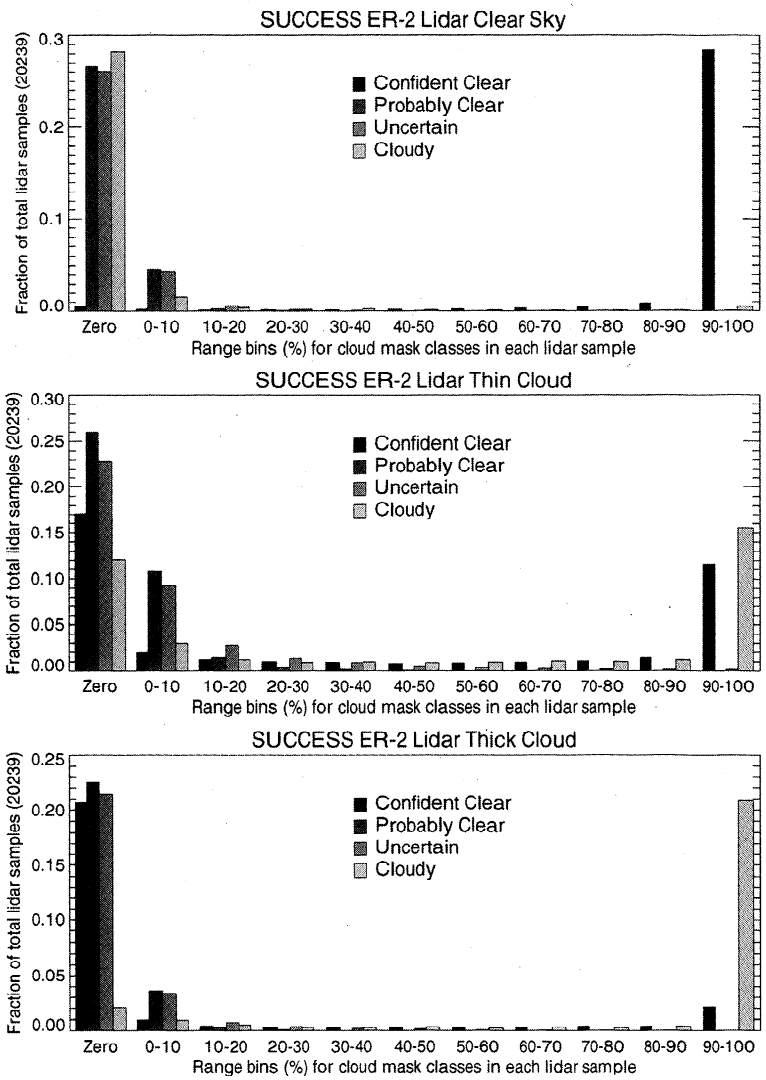

Figure 9. Comparisons between the cloud detection results using MAS and cloud lidar system for 5 days of the SUCCESS experiment. Cloud mask confidence is compared with three lidar categories: no cloud (top), thin cloud (middle), and thick cloud (bottom).

They are suggested approaches and not strict rules. Additional examples are provided by *Ackerman et al.* [1997].

6.1. Clear Scenes Only

Certain applications have little tolerance for cloud or shadow contamination. This is an example of how these applications (e.g., bidirectional reflectance models) might interpret the cloud mask output.

1. Read bit zero to determine if a cloud mask was determined; if zero, no further processing of the pixel is required.
2. If necessary, read bits 3 through 7 to determine scene domain.
3. Read bits 1 and 2; if both bits are not equal to 1, then some tests are suggesting the presence of the cloud, and the pixel is skipped.
4. Read bit 9 to determine if a thin cirrus cloud is present (bit value of zero). An optically thin cirrus cloud may set bit 9 but not be classified as a cloudy scene.
5. Read bit 10 to determine if shadow contamination is present; do not process data if this bit is zero.
6. Daytime algorithms may (depending on application) read bits 32 through 47 to assess potential subpixel contamination or scene variability.

6.2. Clear Scenes With Thin Cloud Correction Algorithms

Some algorithms may be insensitive to the presence of thin cloud or may apply appropriate correction algorithms. This is a suggested application; after launch, minor modifications may be implemented depending on the performance of the cloud-masking algorithm. An example is presented that might be appropriate for normalized difference vegetation index (NDVI).

1. Read bit zero to determine if a cloud mask was determined; if zero, no further processing of the pixel is required.
2. Read bits 3 through 7 to determine if scene domain is appropriate (e.g., land and daytime).
3. Read the confidence flag bits 1 and 2. If cloudy (value of 00), do not process this pixel. A value of 01 for bits 1 and 2 (uncertain) often occurs around cloud edges and retrieving NDVI may not be appropriate with this confidence level. If both bits are equal to 1, then most tests are suggesting clear scenes; proceed with steps 4–7. If confidence bits are 10, then

detailed checking of bits 13 through 25 may be required to determine if the NDVI retrieval should proceed.

4. Read bit 9 to determine if a thin cirrus cloud is present (bit value of zero). An optically thin cirrus cloud may set bit 9 but not be classified as a cloudy scene. Some of the MODIS solar channels are not so sensitive to thin cirrus as the 1.38 μm band (see Figure 1 for a corresponding example using the MAS 1.88 μm channel). If thin cirrus is detected, apply appropriate correction algorithms.

5. Check that reflectance tests (bits 20 and 21) did not detect cloud. Note that a value of zero indicates that either a cloud is present or the test was not run. This test is not run if over snow or solar zenith angles greater than 85°.

6. Read bit 10 to determine if shadow contamination is present. Shadows might bias the NDVI product.

7. Read bits 32 through 47 to assess cloud contamination. This would not be recommended if snow is indicated.

6.3. Cloud Retrieval Algorithms

Use of the cloud mask for cloud scene processing may require a more in-depth analysis than clear-sky applications, as the mask is clear-sky conservative. An approach to interpreting the cloud mask for cloud property retrievals during the day over ocean scenes in non-Sun glint regions is outlined.

1. Read bit zero to determine if a cloud mask was determined; if zero, no further processing of the pixel is required.

2. Read bit 3; if zero, no further processing of the pixel is required (night).

3. Read bits 6 and 7; if 00, then proceed (water).

4. Read bit 4; if zero, then it is a Sun glint region. The user may want to place less confidence on a product retrieval.

5. Read the confidence flag bits 1 and 2. (1) If confident clear (value of 11), read bit 9 to determine if a thin cirrus cloud is present (bit value of zero). An optically thin cirrus cloud may set bit 9 but not be classified as a cloudy scene. If thin cirrus is detected, apply appropriate algorithms or place less confidence on the product retrieval. If bit 9 is 1, then no further processing is required. (2) If both bits are equal to 00, then the scene is cloudy. Check bit 8 for possible heavy aerosol loading. If bit 8 is zero, then the pixel may be aerosol contaminated. In this case, no further processing is necessary or place less confidence on the product retrieval. (3) If confidence is 10 or 01, then detailed checking of bits 13 through 25 may be required to determine if the retrieval algorithm should be executed. For example, if confidence bits are 10 and pixel is in a Sun glint region, additional testing is advised.

6. Check how many tests detected cloud. The greater the number of tests that detected cloud, the more confidence one has in the cloud property product. Note that a value of zero indicates that either a cloud is present or the test was not run.

7. Check spatial variability test results.

8. Read bits 32 through 47 to assess subpixel cloud contamination. This would not be recommended for regions with Sun glint.

7. Summary

The MODIS cloud mask is more than a simple yes/no decision. The cloud mask includes four levels of confidence whether a pixel is clear (bits 1 and 2) as well as the results from different spectral tests. An individual confidence flag is assigned to each single-pixel test and is a function of how close the observation is to the threshold. The individual confidence flags are combined to produce the final cloud mask flag for the output file.

The MODIS cloud mask algorithm is divided into several conceptual domains according to surface type and solar illumination. Each domain defines a processing path through the algorithm, which in turn defines the spectral tests performed and associated thresholds. Different cloud conditions are detected by different tests. Spectral tests which find similar cloud conditions are grouped together. The groups are arranged so that independence between them is maximized, but few, if any, spectral tests are completely independent of all the others.

Example cloud masks from AVHRR and MAS data reveal that most observations have either high confidences ($Q > 0.95$) or very low confidences ($Q < 0.05$) of unobstructed views of the surface. However, there are always those difficult scenes which result in intermediate confidence of the clear sky. These tend to be found at cloud boundaries, or where low clouds are found over water surfaces at night, or over certain land surfaces such as desert or other sparsely vegetated regions. In these cases ($Q > 0.05$ and $Q < 0.95$), spatial and/or temporal continuity tests are conducted.

Initial validation of the cloud mask algorithm has been accomplished with visual inspection of imagery, comparison with surface cloud observations, and comparison with lidar retrievals. While the results show good agreement, it is anticipated that considerable adjustment to the algorithm will be necessary in the first six months after MODIS launch. Routine and reliable production of the MODIS cloud mask is anticipated in late 1998.

Acknowledgments. The authors would like to graciously thank Bryan Baum, Crystal Shaaf, George Riggs, Michael King, Si-Chee Tsay, North Larsen, Jason Li, Chris Sisko, and Yoram Kaufman for their help in the development and testing of the MODIS cloud mask. We would also like to thank Jim Spinhirne and his research group for providing lidar data used in cloud mask validation. This research was funded under NASA grant NAS5-31367. NASA grants NAG5-3193 and NAGW-3318 also contributed to MAS data collection during SUCCESS.

References

Ackerman, S. A., Global satellite observations of negative brightness temperature difference between 11 and 6.7 μm, *J. Atmos. Sci.*, *53*, 2803–2812, 1996.

Ackerman, S. A., Remote sensing aerosols from satellite infrared observations, *J. Geophys. Res.*, *102*, 17,069–17,079, 1997.

Ackerman, S. A., and S. K. Cox, Comparison of satellite and all-sky camera estimates of cloud cover during GATE, *J. Appl. Meteorol.*, *20*, 581–587, 1981.

Ackerman, S. A., and K. I. Strabala, Satellite remote sensing of H_2SO_4 aerosol using the 8–12 μm window region: Application to Mount Pinatubo, *J. Geophys. Res.*, *99*, 18,639–18,649, 1994.

Ackerman, S. A., W. L. Smith, and H. E. Revercomb, The 27–28 October 1986 FIRE IFO cirrus case study: Spectral properties of cirrus clouds in the 8–12 μm window, *Mon. Weather Rev.*, *118*, 2377–2388, 1990.

Ackerman, S. A., K. I. Strabala, W. P. Menzel, R. A. Frey, C. C. Moeller, L. E. Gumley, B. A. Baum, C. Schaaf, and G. Riggs, Discriminating clear sky from cloud with MODIS algorithm theoretical basis document (MOD35), Eos ATBD web site, 125 pp., 1997.

Baum, B. A., T. Uttal, M. Poellot, T. P. Ackerman, J. M. Alvarez, J. Intrieri, D. O'C. Starr, J. Titlow, V. Tovinkere, and E. Clothiaux, Satellite remote sensing of multiple cloud layers, *J. Atmos. Sci.*, *52*, 4210–4230, 1995.

Ben-Dor, E., A precaution regarding cirrus cloud detection from airborne imaging spectrometer data using the 1.38 μm water vapor band, *Remote Sens. Environ.*, *50*, 346–350, 1994.

Frey, R. A., S. A. Ackerman, and B. J. Soden, Climate parameters from satellite spectral measurements, I, Collocated AVHRR and HIRS/2 observations of the spectral greenhouse parameter, *J. Clim.*, *9*, 327–344, 1995.

Gao, B.-C., and A. F. H. Goetz, Cloud area determination from AVIRIS data using water vapor channels near 1 μm, *J. Geophys. Res.*, *96*, 2857–2864, 1991.

Gao, B.-C., A. F. H. Goetz, and W. J. Wiscombe, Cirrus cloud detection from airborne imaging spectrometer data using the 1.38 μm water vapor band, *Geophys. Res. Lett.*, *20*, 301–304, 1993.

Gesell, G., An algorithm for snow and ice detection using AVHRR data: An extension to the APOLLO software package, *Int. J. Remote Sens.*, *10*, 897–905, 1989.

Hall, D. K., G. A. Riggs, and V. V. Salomonson, Development of methods for mapping global snow cover using Moderate Resolution Imaging Spectroradiometer data, *Remote Sens. Environ.*, *54*, 127–140, 1995.

Hutchison, K. D., and K. R. Hardy, Threshold functions for automated cloud analyses of global meteorological satellite imagery, *Int. J. Remote Sens.*, *16*, 3665–3680, 1995.

Inoue, T., A cloud type classification with NOAA 7 split window measurements, *J. Geophys. Res.*, *92*, 3991–4000, 1987.

King, M. D., Y. J. Kaufman, W. P. Menzel, and D. Tanré, Remote sensing of cloud, aerosol, and water vapor properties from the Moderate Resolution Imaging Spectrometer (MODIS), *IEEE Trans. Geosci. Remote Sens.*, *30*, 2–27, 1992.

King, M. D., et al., Airborne scanning spectrometer for remote sensing of cloud, aerosol, water vapor and surface properties, *J. Atmos. Oceanic Technol.*, *13*, 777–794, 1996.

Kriebel, K. T., and R. W. Saunders, An improved method for detecting clear sky and cloudy radiances from AVHRR data, *Int. J. Remote Sens.*, *9*, 123–150, 1988.

Leprieur, C., Y. H. Kerr, and J. M. Pichon, Critical assessment of vegetation indices from AVHRR in a semi-arid environment, *Int. J. Remote Sens.*, *17*, 2549–2563, 1996.

McClain, E. P., Evaluation of CLAVR Phase-I algorithm performance, final report, *Rep. 40-AANE-201-424*, U.S. Dep. of Commerce/NOAA/NESDIS, Washington, D. C., 1993.

Menzel, W. P., D. P. Wylie, and K. I. Strabala, Trends in global cirrus inferred from four years of HIRS data, paper presented at the Technical Proceedings of the Seventh International TOVS Study Conference, Igls, Austria, 10–16 February, 1993.

Pinty, B., and M. M. Verstraete, GEMI: A non-linear index to monitor global vegetation from satellites, *Vegetation*, *101*, 15–20, 1992.

Rizzi, C. Serio, G. Kelly, V. Tramutoli, A. McNally, and V. Cuomo, Cloud clearing of infrared sounder radiances, *J. Appl. Meteorol.*, *33*, 179–194, 1994.

Rossow, W. B., Measuring cloud properties from space, A review, *J. Clim.*, *2*, 201–213, 1989.

Rossow, W. B., and L. C. Garder, Cloud detection using satellite measurements of infrared and visible radiances for ISCCP, *J. Clim.*, *6*, 2341–2369, 1993a.

Rossow, W. B., and L. C. Garder, Validation of ISCCP cloud detections, *J. Clim.*, *6*, 2370–2393, 1993b.

Rossow, W. B., A. W. Walker, and L. C. Garder, Comparison of ISCCP and other cloud amounts, *J. Clim.*, *6*, 2394–2418, 1993.

Saunders, R. W., and K. T. Kriebel, An improved method for detecting clear sky and cloudy radiances from AVHRR data, *Int. J. Remote Sens.*, *9*, 123–150, 1988.

Seze, G., and W. B. Rossow, Time-cumulated visible and infrared radiance histograms used as descriptors of surface and cloud variations, *Int. J. Remote Sens.*, *12*, 877–920, 1991.

Smith, W. L., An improved method for calculating tropospheric temperature and moisture profiles from satellite radiometer measurements, *Mon. Weather Rev.*, *96*, 387, 1968.

Smith, W. L., and C. M. R. Platt, Comparison of satellite-deduced cloud heights with indications from radiosonde and ground-based laser measurements, *J. Appl. Meteorol.*, *17*, 1796–1802, 1978.

Smith, W. L., H. M. Woolf, S. J. Nieman, and T. H. Achtor, ITPP-5—The use of AVHRR and TIGR in TOVS Data Processing, paper presented at the Technical Proceedings of the Seventh International TOVS Study Conference, Igls, Austria, 10–16 February, 1993.

Spinhirne, J. D., and W. D. Hart, Cirrus structure and radiative properties from airborne lidar and spectral radiometer observations, *Mon. Weather Rev.*, *118*, 2329, 1990.

Soden, B. J., and F. P. Bretherton, Upper tropospheric relative humidity from the GOES 6.7 μm channel: Method and climatology for July 1987, *J. Geophys. Res.*, *98*, 16,669–16,688, 1993.

Stowe, L. L., E. P. McClain, R. Carey, P. Pellegrino, G. Gutman, P. Davis, C. Long, and S. Hart, Global distribution of cloud cover derived from NOAA/AVHRR operational satellite data, *Adv. Space Res.*, *11*, 51–54, 1991.

Stowe, L. L., S. K. Vemury, and A. V. Rao, AVHRR clear sky radiation data sets at NOAA/NESDIS, *Adv. Space Res.*, *14*, 113–116, 1994.

Strabala, K. I., S. A. Ackerman, and W. P. Menzel, Cloud properties inferred from 8–12 μm data, *J. Appl. Meteorol.*, *33*, 212–229, 1994.

Wylie, D. P., and W. P. Menzel, Two years of cloud cover statistics using VAS, *J. Clim. Appl. Meteorol.*, *2*, 380–392, 1989.

Wylie, D. P., W. P. Menzel, H. M. Woolf, and K. I. Strabala, Four years of global cirrus cloud statistics using HIRS, *J. Clim.*, *7*, 1972–1986, 1994.

S. A. Ackerman, R. A. Frey, L. E. Gumley, W. P. Menzel, C. C. Moeller, and K. I. Strabala, Space Science and Engineering Center/CIMSS, University of Wisconsin-Madison, 1225 West Dayton Street, Madison, WI 53706. (e-mail: paul.menzel@ssec.wisc.edu)

(Received December 2, 1997; revised September 25, 1998; accepted September 28, 1998.)